

END-TO-END BEAM SIMULATIONS FOR THE MSU RIA DRIVER LINAC*

X. Wu[†], M. Doleans, D. Gorelov, Q. Zhao, T. L. Grimm, F. Marti and R. C. York,
National Superconducting Cyclotron Laboratory, Michigan State University, E. Lansing,
MI 48824, USA

Abstract

The Rare Isotope Accelerator (RIA) [1] driver linac proposed by Michigan State University (MSU) will use a 10th sub-harmonic based, superconducting, cw linac to accelerate light and heavy ions to final energies of ≥ 400 MeV/u with beam powers of 100 to 400 kW. The driver linac uses for acceleration superconducting quarter-wave, half-wave, and six-cell elliptical cavities with frequencies ranging from 80.5 MHz to 805 MHz, and for transverse focusing superconducting solenoids and room temperature quadrupoles. For the heavier ions, two stages of charge-stripping and multiple-charge-state acceleration will be used to meet the beam power requirements and to minimize the requisite accelerating voltage. End-to-end, three-dimensional (3D), beam dynamics simulations from the Front End to the output of the driver linac have been performed. These studies include a 3D analysis of multi-charge-state beam acceleration, evaluation of transverse misalignment and rf errors on the machine performance, and modeling of the charge-stripping foils and stripping-chicane performance. The results of these beam dynamics studies will be presented, and further planned beam dynamics studies will be discussed.

INTRODUCTION

RIA beam dynamics studies [2,3] have been performed at Michigan State University since 1999 as part of an overall effort to establish a comprehensive design for RIA and in support of the on-going Superconducting Radio Frequency (SRF) R&D program. To meet the beam power (≤ 400 kW) specification, multi-charge state beam acceleration for heavy ions is required. To meet beam loss criteria ($\leq 10^{-4}$) for hand-on maintenance, adequate acceptances and limited emittance growths must be achieved. The MSU RIA driver lattice design [4] was predominantly motivated by the minimization of technical risk and maximization of simplicity, leading to higher probability of achieving performance and increased operational efficiencies. The 10th sub-harmonic or 80.5 MHz was chosen, compared to 14th sub-harmonic or 57.5 MHz proposed by ANL [5], as the lowest linac frequency to significantly reduce microphonics in the first segment of the Superconducting Linac (SCL), allowing a simple solution utilizing a mechanical damper and modest rf while avoiding the VCX tuner reliability concerns. The design requires only three rf frequencies and six SRF cavity types for the driver linac.

*Work supported by MSU and DOE.

[†]xwu@nsl.msue.edu

Figure 1 shows the Rare Isotope Accelerator (RIA) driver linac layout that is being evaluated at MSU. A folded MSU RIA driver linac option also exists by bending the beam 180° in the 2nd charge-stripping chicane. It consists of a room temperature Front End, and three segments of superconducting rf linac, separated by two charge-stripping sections that provide a cost-effective method of achieving the final beam energy for a wide range of ions from proton to uranium. A beam switchyard will deliver up to 400 MeV/u ion beams to the Isotope Separation On Line (ISOL) and Particle Fragmentation (PF) target area. The RIA driver linac will be operated in a continuous-wave (cw) mode, effectively providing a 100% duty factor.

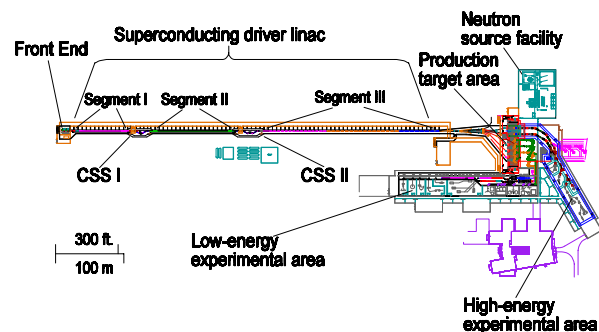


Figure 1: Layout of the MSU RIA driver linac.

End-to-end beam simulations were performed to quantify the driver linac performance and evaluate the full effects of alignment and rf errors through all three segments of the driver linac, given a realistic initial input beam from the ECR ion source. A model of the charge stripping foil including the effects of multiple scattering, energy loss and straggling, and variation in foil thickness was also included in the simulations. Since the multi-charge state beam acceleration for heavy ions [6] is the most challenging, our end-to-end simulations assumed an initial beam consisting of a two-charge state ^{238}U beam from the ECR going through two charge-stripping targets during acceleration in RIA driver linac. Charge states of 28+ and 29+, 71+ to 75+, and 87+ to 89+ will be accelerated in Segments I, II and III, respectively.

Various computer codes were used for beam dynamics studies. The simulations for the Front End were done primarily using PARMELA and PARMTEQ to include space-charge effects. LANA [7] was used for the longitudinal beam dynamics studies, 6-D phase space particle tracking, and rf error analysis in the SCL segments. DIMAD [8] and COSY INFINITY were used to study the transverse focusing structure, beam matching,

and transverse misalignment and high-order aberration correction schemes. The charge-stripping foil model was based on simulation results from TRIM. Collaborations between MSU, Lawrence Berkeley National Laboratory (LBNL) and Los Alamos National Laboratory (LANL) have been initiated to provide an additional simulation tool based upon PARMTEQm and IMPACT.

END-TO-END BEAM SIMULATIONS FOR THE RIA DRIVER LINAC

Initial Beam and RIA Front End Simulations

The MSU RIA driver linac Front End is comprised of several ECR ion sources, achromatic charge-selection sections, a Low Energy Beam Transport (LEBT), a Radio Frequency Quadrupole (RFQ), and a Medium Energy Beam Transport (MEBT) system. The objective is to accelerate a wide range of selected single- or multi-charge state beams from the ECR to about 300 keV/u and provide the required longitudinal bunching and transverse matching into the following SRF linac segments. The LEBT uses a Multi-Harmonic Buncher (MHB) and a Velocity Equalizer (VE) to efficiently prebunch the selected dc beam for injection into the 80.5 MHz RFQ. Magnetic and electrostatic quadrupole magnets and solenoid magnets are used for transverse focusing and matching.

As part of RIA collaborations, the VENUS ECR ion source has been developed at LBNL as a possible ion source. Recently, a 3 μA ^{27+}Bi from VENUS [9] has been measured with a normalized rms emittance of $\sim 0.08\pi$ mm-mrad, which is comparable with the input beam required for RIA. The initial phase spaces of a two-charge state ^{238}U beam at the entrance, shown in Figure 2, are based on the VENUS emittance measurement results and used in our end-to-end beam simulations. The assumed total two-charge state beam intensity was 8 μA to achieve a beam power of 400 kW.

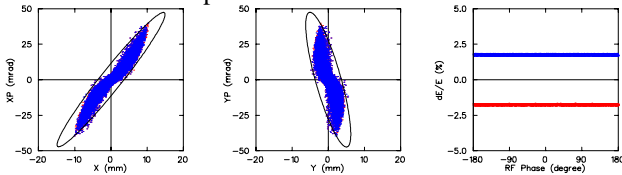


Figure 2: Horizontal (left), vertical (middle), and longitudinal (right) phase spaces of a two charge-state uranium beam at the entrance of the RIA Front End.

The two-charge-state uranium beam was simulated using PARMELA and PARMTEQ through the LEBT, RFQ and MEBT [10], and the phase spaces at the exit of the RIA Front End are shown in Figure 3. The longitudinal and transverse normalized emittances (99.5%) for a two charge-state uranium beam entering SCL Segment I will be 1.2π keV/u-ns and 0.9π mm-mrad, with rms values of 0.1π keV/u-ns and 0.09π mm-mrad. Our previous simulations [2] used a matched 4D water bag for the beam distribution. For the experimentally-

based beam distribution used here, only the 99.5% transverse emittances are relatively larger. No significant space-charge effects were observed with the assumed beam intensity in our simulation. The small transverse emittance growth in the Front End is primarily due to the offset of the two charge states in transverse phase spaces.

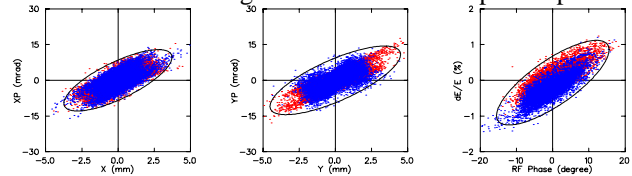


Figure 3: Horizontal (left), vertical (middle), and longitudinal (right) phase spaces of a two charge-state uranium beam at the exit of the RIA Front End.

Misalignment and RF Errors

The misalignment of SRF cavities and focusing elements lead to distortion of the beam centroid orbit, envelope growth, and transverse and longitudinal emittance growth, due mainly to the non-linear field distribution in the SRF cavities. These effects are especially strong in Segment I where the beam energy is low. Orbit correction is necessary to prevent significant emittance growth and possible beam loss. Since the transverse de-focusing due to the SRF cavities is much weaker than the focusing provided by the solenoids and quadrupoles, the impact on the beam transverse motion from the rf field errors is limited, and the SRF cavities are much less sensitive to the alignment errors. However, the rf field errors have a significant effect on the longitudinal emittance growth. Previous beam dynamics studies [11] of SCL segments have established the alignment and rf error tolerances listed in Tables 1 and 2, which were used in the end-to-end simulations. The misalignment includes all SRF cavities and focusing elements assuming a Gaussian distribution ($\pm 2\sigma$), while a uniform distribution was used for rf errors. The correction of the beam centroid orbit was done using beam position monitors between cryomodules, dipole windings in the solenoids of Segments I and II, and dipole corrector magnets at quadrupoles in Segment III.

Table 1: Alignment Tolerances

RIA driver linac Segment	Misalignment $\sigma_{x,y}$ (mm)	
	SRF Cavity	Focusing element
I	1.0	0.5
II	1.0	0.5
III	1.0	1.0

Table 2: RF Error Tolerances

RIA Driver Linac Segment	SRF Cavity RF Errors	
	Phase	Amplitude
I	$\pm 0.25^\circ$	$\pm 0.25\%$
II	$\pm 0.50^\circ$	$\pm 0.50\%$
III	$\pm 0.50^\circ$	$\pm 0.50\%$

Charge-Stripping Foil Modeling

To achieve the required beam energy, heavy ions like uranium will pass through two charge-stripping foils to increase the acceleration efficiency. The model used for stripping foils is based on simulation results from the code TRIM that include elastic and inelastic scattering, and energy loss for ionization. A small transverse beam spot (~3 mm) and short bunch length (~8°) on both charge-stripping targets were obtained to minimize the beam transverse and longitudinal emittance increase due to multiple scattering and energy straggling in the stripping material.

Carbon foils were used in our end-to-end simulations. In addition to multiple scattering and energy straggling, foil thickness variation also contributed to the beam emittance growth; ±5% was assumed for the foil thickness variation. Due to the high beam energy at the end of Segment II, a much thicker foil was required for the 2nd charge-stripper. Table 3 gives the carbon foil parameters for the RIA driver linac. The estimated emittance growth will not significantly degrade the overall performance. Experimental work has been performed at NSCL using the beam from the K1200 Superconducting Cyclotron to explore the feasibility of carbon and other foils, and tests using diamond foils and lithium jets as charge-strippers for RIA are in progress in Argonne National Laboratory (ANL) and other institutes.

Table 3: Charge-Stripping Foils Parameters

Stripping location	Stripping Energy (MeV/u)	Ave. Foil Thickness (μm)	Emittance Growth	
			Trans.	Longi.
1 st	11.9	1.8	~ 20%	~ 65%
2 nd	89.2	64.4	~ 45%	~103%

SCL Segment I – Low β Section

Segment I of the RIA diver linac will be used to accelerate two-charge state Uranium beams to ~12 MeV/nucleon. It uses two types of Quarter Wave Resonators (QWR) with β_{opt} of 0.041 and 0.085 operating at 80.5 MHz with peak surface electric field (E_p) of 16.5 MV/m and 20 MV/m, respectively. The focusing lattice will consist of 76 solenoids, each having independent dipole windings to provide horizontal and vertical orbit corrections. The beam position monitors are located in the warm regions between cryomodules.

Figure 4 shows the transverse and longitudinal phase spaces at the end of Segment I using LANA with an initial phase space shown in Figure 3 without alignment or rf errors. Figure 5 shows the evolution of the normalized (rms) emittance. The total longitudinal emittance displays an oscillatory behavior along Segment I because the two charge states of uranium perform coherent oscillations in longitudinal phase space due to their different charge-to-mass ratios. The transverse and longitudinal emittance (rms) growth factors for the perfect lattice of Segment I were ~1.0, and ~1.35, respectively. The calculated longitudinal acceptance to emittance ratio at the entrance of Segment I was 2.9:1.

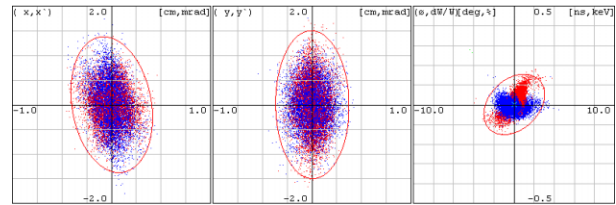


Figure 4: Horizontal (left), vertical (middle), and longitudinal (right) phase spaces of a two charge-state uranium beam at the end of Segment I.

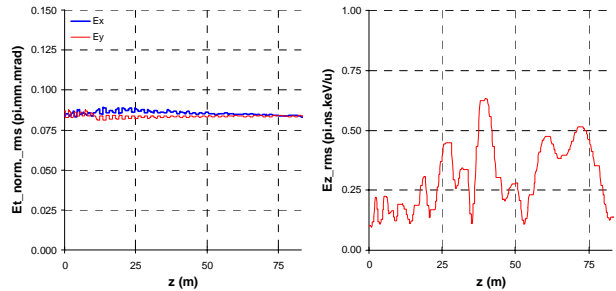


Figure 5: Transverse (left), and longitudinal (right) beam emittance (rms) for a two charge-state uranium beam in Segment I without errors.

Beam simulations using LANA were performed to investigate the influence of the transverse misalignment and rf phase and amplitude errors on beam quality. With the alignment and rf error tolerances listed in Tables 1 and 2, and alignment correction applied with 100 random seeds, no beam loss was observed in Segment I. Confidence plots for the transverse and longitudinal emittances (rms) at the end of Segment I are shown in Figure 6. With 90% confidence, the transverse and longitudinal emittance (rms) growth factor due to combined transverse misalignment and rf errors in Segment I are ~ 1.8 and 4.3, respectively. The maximum beam envelope in Segment I is ~10.4 mm from all 100 random seed runs. With an SRF cavity radial aperture of 15 mm, the ratio of aperture to beam envelope is ~1.4:1 with errors, indicating that Segment I has adequate transverse acceptance. Further improvement could be achieved via transverse collimation of the beam tails in the MEBT.

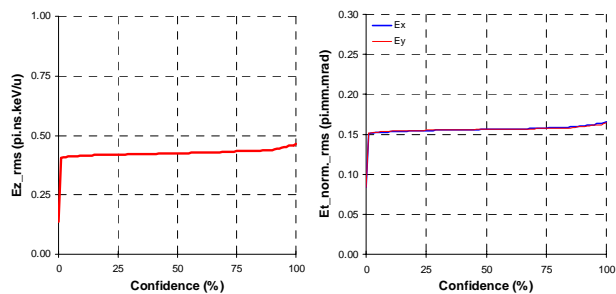


Figure 6: Transverse (left) and longitudinal (right) rms emittances at the end of Segment I for multi-charge uranium beam with errors vs. statistical confidence.

SCL Segment II – Medium β Section

Segment II of the RIA driver linac will accelerate the multi-charge uranium beam (71+~75+) from ~12 MeV/u to about 90 MeV/u. It uses a total of 208 superconducting Half-Wave cavities in 26 cryomodules, operating at a frequency of 322 MHz with a design peak surface electric field of 25 MV/m. The transverse focusing will use 2 superconducting solenoids per cryomodule for a total of 52 focusing elements. Each solenoid will also have independent dipole windings to provide horizontal and vertical orbit corrections. The beam position monitors used for corrections are located in the warm region between cryomodules as for Segment I.

Figure 7 shows the transverse and longitudinal phase spaces without alignment or rf errors at the end of Segment II for the five charge-state uranium ion beam continued from Segment I. Figure 8 shows the evolution of the normalized transverse and longitudinal (rms) emittance in Segment II. Due to the higher beam energy in Segment II, the beam's longitudinal motion is more adiabatic and matching between cavities and cryomodules is easier. No transverse and only a small longitudinal emittance growth were observed. The transverse and longitudinal emittance (rms) growth factors for the perfect lattice of Segment II are ~1.0, and ~1.3, respectively.

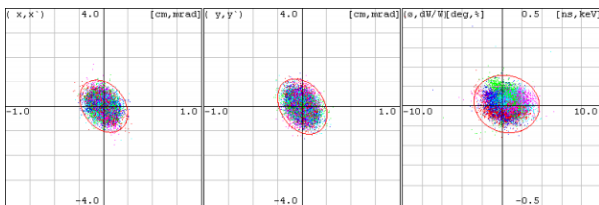


Figure 7: Horizontal (left), vertical (middle), and longitudinal (right) phase spaces of a five charge-state uranium beam at the end of Segment II.

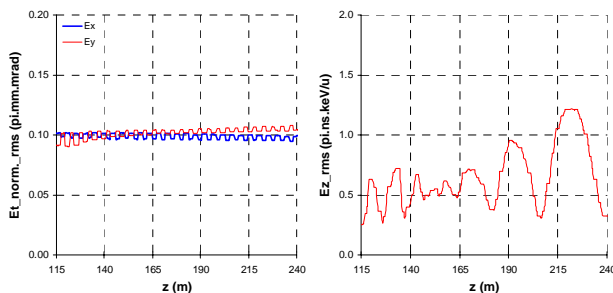


Figure 8: Transverse (left), and longitudinal (right), beam emittance (rms) for a multi-charge state uranium beam in Segment II without errors.

The transverse misalignment and rf errors in Segment II were then included to continue beam simulations from Segment I using LANA for 100 random seeds. As in Segment I, no beam loss was observed in Segment II. Confidence plots for the transverse and longitudinal emittance (rms) at the end of Segment II are shown in Figure 9. With 90% confidence, the transverse and longitudinal emittance (rms) growth factors in Segment II

with transverse misalignment and rf errors were increased to ~ 1.1 and 1.8, respectively. The sensitivities to misalignment and rf errors are significantly less than those in Segment I. The maximum beam envelope in Segment II is ~9.6 mm from all 100 random seed runs. With an SRF cavity radial aperture of 15 mm, the ratio of aperture to beam envelope will be about 1.6:1 with errors and after orbit correction, indicating that Segment II also has adequate transverse acceptance. Since the longitudinal acceptance at the entrance of Segment II is ~ 20 π keV/u-n, the beam longitudinal emittance (99.5%) of ~ 6.2 π keV/u-n at the entrance of Segment II from our simulations leads to an adequate longitudinal acceptance to emittance ratio of 3.2:1.

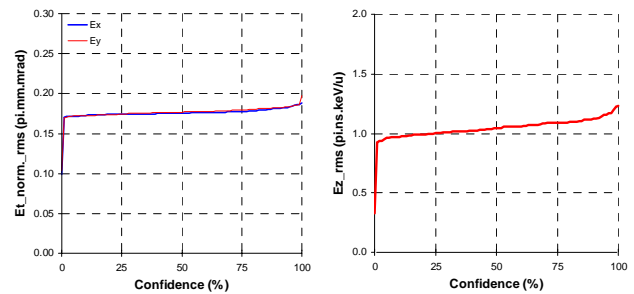


Figure 9: Transverse (left) and longitudinal (right) rms emittances at the end of Segment II for multi-charge uranium beam with errors vs. statistical confidence.

SCL Segment III – High β Section

Segment III will accelerate the multi-charge uranium beam (87+~89+) to the final energy of 400 MeV/u. It uses a total of 164 6-cell SRF elliptical cavities in 41 cryomodules, operating at a frequency of 805 MHz with a design peak surface electric field of 32.5 MV/m. The focusing lattice will use in each inter-cryostat warm region a room temperature quadrupole doublet with a pair of corrector magnets to provide horizontal and vertical orbit corrections.

Figure 10 shows the transverse and longitudinal phase space without alignment or rf errors at the end of Segment III for the multi-charge state uranium beam continued from Segment II. Figure 11 shows the evolution of the normalized (rms) emittance evolutions in Segment III. The transverse and longitudinal emittance (rms) growth factors for the perfect lattice of Segment III are ~1.0, and ~1.27, respectively.

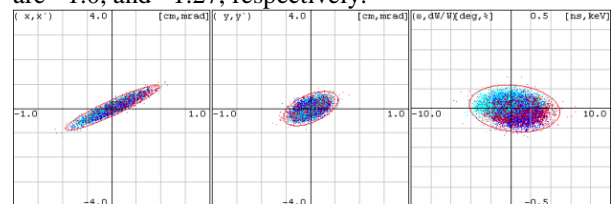


Figure 10: Horizontal (left), vertical (middle), and longitudinal (right) phase spaces of a multi-charge uranium beam at the end of Segment III without alignment or rf errors.

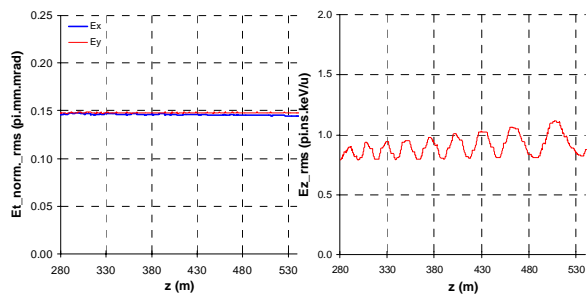


Figure 11: Transverse (left) and longitudinal (right) beam emittance (rms) for a multi-charge state uranium beam in Segment III without errors.

Beam simulations from Segment II were continued using LANA with alignment and rf errors in Segment III. Since the orbit correctors were paired with the relatively weak focusing quadrupoles with a beam position monitor in each focusing cell, the orbit correction was much more effective than that for Segments I and II. No beam loss was observed in Segment III. The confidence plots for the transverse and longitudinal emittances (rms) at the end of Segment III are shown in Figure 12. The alignment and rf errors have no significant impact on lattice performance in Segment III. With 90% confidence, the transverse and longitudinal emittance (rms) growth factors have only been increased to ~ 1.05 and 1.3 , respectively, due to transverse misalignment and rf errors. The maximum beam envelope in Segment III is ~ 12 mm from all 100 random seed runs. Since the elliptical cavities used in Segment III have a much larger radial aperture (38.5mm), the ratio of aperture to beam size was about 3.2:1 with errors. Assuming a focusing quadrupole radial aperture of 25mm, the ratio of aperture to beam size with errors is about 2.1:1, indicating that Segment III also has adequate transverse acceptance. Compared to 345 MHz Triple-spoke cavities, the 805 MHz elliptical cavities used in Segment III have a smaller longitudinal acceptance of $\sim 115 \pi$ keV/u-ns mainly due to the higher frequency. The longitudinal emittance (99.5%) of $\sim 20.2\pi$ keV/u-ns at the entrance of Segment III was obtained from our end-to-end beam simulations with errors, leading to an adequate longitudinal acceptance to emittance ratio of 5.7:1.

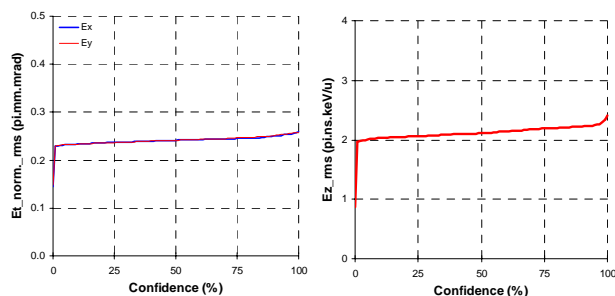


Figure 12: Transverse (left) and longitudinal (right) rms emittances at the end of Segment III for a multi-charge uranium beam with errors vs. statistical confidence.

SUMMARY AND CONCLUSIONS

End-to-end beam simulation results with experimentally-based input beams including alignment and rf errors and charge-stripping foils, indicate that the MSU 10th sub-harmonic RIA driver linac option has adequate transverse and longitudinal acceptances to achieve the beam power and beam loss requirements for RIA even for the most challenging multi-charge state heavy ion beams. The alignment and rf error tolerances are reasonable and have been shown to be achievable from past experience. Further beam dynamics studies will include developing an automated SRF cavity tuning procedure for multi-charge beam acceleration, performing lattice element failure analysis, and establishing failure tolerances to meet the high availability desired for RIA. Advantage will be taken of the parallel computing capabilities of PARTEQm and IMPACT currently being developed at LBNL and LANL for beam simulations.

REFERENCES

- [1] C. W. Leemann, "The Rare-Isotope Accelerator (RIA) Facility Project", proceedings of the XXth Int. Linac Conference, Monterey, California, 2000.
- [2] D. Gorelov, T. Grimm, W. Hartung, F. Marti, H. Podlech, X. Wu and R. C. York, "Beam Dynamics Studies at NSCL of the RIA Superconducting Driver Linac", proceedings of EPAC 2002, Paris, France, 2002.
- [3] X. Wu, "Beam Dynamics Studies for RIA at Michigan State University", RIA R&D Workshop, Bethesda, Maryland, August 2003.
- [4] "The Rare Isotope Accelerator (RIA) at Michigan State University", RIA R&D Workshop, Bethesda, Maryland, August 2003.
- [5] P. N. Ostroumov, "Design Features of high-intensity medium-energy superconducting heavy-ion linac", proceedings of the XXI Linac Conference, Gyeongju, Korea, August 2002.
- [6] P. N. Ostroumov et al., "Multiple-charge Beam Dynamics in an Ion Linac", proceedings of the XX Linac Conference, Monterey, CA, August 2000.
- [7] D. Gorelov, and P. N. Ostroumov, "Application of LANA Code for Design of Ion Linac", EPAC'96, Sitges, June 1996
- [8] R. Servranckx, K. Brown, L. Schachinger, and D. Douglas, "User's Guide to the Program Dimad", SLAC Report 285, UC-28, May 1985.
- [9] D. Leitner, RIA Facility Workshop, East Lansing, MI, March 2004.
- [10] Q. Zhao, et al., "Design Improvement of the RIA 80.5 MHz RFQ", these proceedings.
- [11] X. Wu, D. Gorelov, T. Grimm, W. Hartung, F. Marti, and R.C. York, "The Beam Dynamics Studies of Combined Misalignment and RF Errors for RIA", proc. of PAC 2003, Portland, Oregon, 2003.